Available online at www.sciencedirect.com
SCIENCE DIRECT®
Journal of Computational Physics 190 (2003) 501–522
JOURNAL OF COMPUTATIONAL PHYSICS
www.elsevier.com/locate/jcp

Numerical modelling of the two-dimensional Fourier transformed Vlasov–Maxwell system

Bengt Eliasson

Theoretische Physik IV, Ruhr-Universität Bochum, D-44780 Bochum, Germany

Received 9 January 2003; received in revised form 21 May 2003; accepted 27 May 2003

Abstract

The two-dimensional Vlasov–Maxwell system, for a plasma with mobile, magnetised electrons and ions, is investigated numerically. A previously developed method for solving the two-dimensional electrostatic Vlasov equation, Fourier transformed in velocity space, for mobile electrons and with ions fixed in space, is generalised to the fully electromagnetic, two-dimensional Vlasov–Maxwell system for mobile electrons and ions. Special attention is paid to the conservation of the divergences of the electric and magnetic fields in the Maxwell equations. The Maxwell equations are rewritten, by means of the Lorentz potentials, in a form which conserves these divergences. Linear phenomena are investigated numerically and compared with theory and with previous numerical results.

Keywords: Vlasov equation; Maxwell equation; Divergence problem

1. Introduction

For many decades, methods of solving numerically the Vlasov equation have been developed, including methods based on Hermite and Fourier expansions [1,7] and methods based on the time splitting scheme [6], which has been generalised to higher dimensions for simulations of magnetised plasma [5,21]. Convective schemes have also been developed for the collisional Boltzmann equation [12], and a conservative scheme has been developed for the one-dimensional Vlasov equation [13].

A problem with the Vlasov equation is its tendency of becoming oscillatory in velocity space, potentially giving rise to recurrence effects where parts of the initial condition artificially reappear in the numerical solution [1,6]. Several approaches of minimising effects due to the recurrence phenomenon have been developed: In the original time-splitting scheme [6] smoothing operators are applied to the numerical solution so that the finest structures are damped out on the numerical grid. A filtered method based on a convolution by a Gaussian function in velocity space has been developed for the Fourier–Fourier method [19], and for the time-splitted Fourier–Fourier method [18]. In the filtered method, the Vlasov equation is

E-mail address: bengt@tp4.ruhr-uni-bochum.de.

0021-9991/$ - see front matter
doi:10.1016/S0021-9991(03)00295-X

transformed into an equation with smoother solutions. Another approach was the Fourier–Fourier method, where the Vlasov equation is Fourier transformed both in $\mathbf{x}$ and $\mathbf{v}$ space [1]. Taking up this line of ideas, methods to solve the electrostatic Vlasov–Poisson system, Fourier transformed analytically in velocity space, was developed for the cases of one velocity and one spatial dimension [10] and for two velocity and two spatial dimensions [11], and where the problem with filamentation was solved by devicing outflow boundary conditions in the Fourier transformed velocity space; the outflow of information in the Fourier transformed velocity space represents a dissipation of information in velocity space. In the present article, the previously developed method for the two-dimensional Vlasov equation [10] for electrons in magnetized plasma is extended to include the fully electromagnetic treatment of the Maxwell equation together with the two-dimensional Vlasov equations for magnetised electrons and ions, making it possible to study numerically the non-linear interactions between electron and ion Bernstein modes, electromagnetic X waves, and upper and lower hybrid waves, etc.

Mathematically, moments in velocity space are converted to evaluation operators in the Fourier transformed velocity space. Therefore, charge and current densities are in the Fourier transformed velocity space are calculated by means of evaluations (instead of moments) of the Fourier transformed particle distribution functions and of its first derivatives, at the origin of the Fourier transformed velocity space.

In the solution of the Maxwell equations, special attention is paid to the divergence problem for the electric and magnetic fields. In the Maxwell equations, the equations for the divergences of the electric and magnetic fields have the twofold properties of being both initial conditions to the remaining equations, and of being conserved quantities of the Maxwell equations. These two properties may not be carried over to a discretised version of the Maxwell equations. Artificial positive and negative charges may be deposited on the numerical grid by the numerical scheme. The charges do not move and may therefore be regarded as infinitely massive [29]. This problem has been known for a long time, and special numerical methods have been developed to avoid the problem, such as finite-difference time-domain (FDTD), finite-volume time-domain (FVTD), and finite-element time-domain (FETD) methods; see [9] and references therein. We mention the following methods used for solving the Maxwell equation together with the Vlasov equation: [8] developed a current-conserving particle-mesh scheme for the relativistic Vlasov–Maxwell system. Ref. [23] (see also [3]) formulates the problem in terms of the electrodynamic potentials, and uses the Coulomb gauge ($\mathbf{\nabla}_{\mathbf{x}} \cdot \mathbf{A} = 0$) for the vector potential, and the numerical scheme is formulated so that the continuity equation for the currents and charges need not be fulfilled exactly. Ref. [22] adds a "pseudo current" term to the Ampère law, which diffuses away errors in the divergence of $\mathbf{E}$, and where a parabolic equation has to be solved. Ref. [2] reformulated the Maxwell equations into a constrained system, using Lagrange multipliers associated with the divergence conditions and solved the resulting system with a finite element method. [17] proposed the least-squares finite element method (LSFEM) for the treatment of spurious solutions in the numerical solution of the Maxwell equations.

The Vlasov equation is in the present article advanced in time using the fourth-order Runge–Kutta method, and we wish to invoke the Maxwell equation into this scheme while still conserving the divergences of the electric and magnetic fields. This is performed by using the electrodynamic potentials together with the Lorentz condition, giving rise to Lorentz inhomogeneous wave equations. These are written in a form which ensures that the divergences of the electromagnetic fields are fulfilled up to the local truncation error of the numerical scheme, without requiring that the continuity equation for the currents and charges is fulfilled exactly. To our knowledge, this is a new approach which we have not found in earlier literature.

We think that the method presented here for solving the Vlasov–Maxwell system can be suitable for solving basic non-linear problems in plasma physics. Together with the Fourier transform technique in velocity space [which is motivated in Section 2.2], we are using pseudo-spectral methods for approximating derivatives in space, and fourth-order compact schemes to approximate derivatives in the Fourier transformed velocity space, and the standard fourth-order Runge–Kutta scheme to advance the system in time.

The use of high-order methods should make it possible to solve the system with relatively few sampling points, and thereby reduce the need for computer memory, etc. We point out that the method is still restricted to periodic boundary conditions in space, and that the generalisation to open boundaries in space is an unsolved problem.

The outline of the article is as follows. We state the three-dimensional Vlasov–Maxwell system in Section 2 where the Fourier transform technique is discussed in general, as well as the conservation of divergences ion the Maxwell equations and the Lorentz potentials used. In Section 4 the Vlasov–Maxwell system is reduced to two spatial and velocity dimensions and prepared for numerical simulations by scaling of variables, discretisation, etc. The numerical examples in Sections 4.4 and 4.5 checks how well the numerical scheme conserves invariants of the Vlasov–Maxwell system, and compare simulations of electromagnetic electron and ion X waves with dispersion laws obtained from linear fluid theory and kinetic theory. Finally, conclusions are drawn in Section 5.

2. The three-dimensional Vlasov–Maxwell system

The non-relativistic *Vlasov equation*

$$\frac{\partial f_\alpha}{\partial t} + \mathbf{v}\cdot\nabla_{\mathbf{x}} f_\alpha + \frac{\mathbf{F}_\alpha}{m_\alpha}\cdot\nabla_{\mathbf{v}} f_\alpha = 0, \tag{1}$$

where the nabla operators $\nabla_{\mathbf{x}}$ and $\nabla_{\mathbf{v}}$ denote differentiation with respect to $\mathbf{x}$ and $\mathbf{v}$, respectively, and where the *Lorentz force* is

$$\mathbf{F}_\alpha = q_\alpha[\mathbf{E} + \mathbf{v}\times(\mathbf{B} + \mathbf{B}_{\text{ext}})] \tag{2}$$

describes the evolution of the distribution function f_α of electrically charged particles of type α (e.g., "electrons" or "singly ionised oxygen ions"), each particle having the *electric charge* q_α and *mass* m_α. Here, the magnetic field is separated into two parts, where $\mathbf{B}_{\text{ext}}$ is an external magnetic field (e.g., the Earth's geomagnetic field), and $\mathbf{B}$ is the self-consistent part of the magnetic field, created by the plasma. One Vlasov equation is needed for each species of particles.

The particles interact via the electromagnetic field. The *charge* and *current densities*, ρ and $\mathbf{j}$, act as sources of self-consistent electromagnetic fields according to the *Maxwell equations*

$$\nabla_{\mathbf{x}}\cdot\mathbf{E} = \frac{\rho}{\varepsilon_0}, \tag{3}$$

$$\nabla_{\mathbf{x}}\cdot\mathbf{B} = 0, \tag{4}$$

$$\nabla_{\mathbf{x}}\times\mathbf{E} = -\frac{\partial\mathbf{B}}{\partial t}, \tag{5}$$

$$\nabla_{\mathbf{x}}\times\mathbf{B} = \mu_0\mathbf{j} + \frac{1}{c^2}\frac{\partial\mathbf{E}}{\partial t}, \tag{6}$$

where c is the *speed of light*, ε_0 is the *electric vacuum permittivity* and μ_0 is the *magnetic vacuum permeability*. The charge and current densities are related to the *particle number densities* n_α and *mean velocities* $\mathbf{v}_\alpha$ as

$$\rho = \sum_\alpha q_\alpha n_\alpha \tag{7}$$

and

$$\mathbf{j} = \sum_{\alpha} q_\alpha n_\alpha \mathbf{v}_\alpha, \tag{8}$$

respectively, and where the particle number densities and mean velocities are obtained as moments of the particle distribution functions, as

$$n_\alpha(\mathbf{x}, t) = \int_{-\infty}^{\infty} f_\alpha(\mathbf{x}, \mathbf{v}, t)\, \mathrm{d}^3 v \tag{9}$$

and

$$\mathbf{v}_\alpha(\mathbf{x}, t) = \frac{1}{n_\alpha(\mathbf{x}, t)} \int_{-\infty}^{\infty} \mathbf{v} f_\alpha(\mathbf{x}, \mathbf{v}, t)\, \mathrm{d}^3 v, \tag{10}$$

respectively.

The Vlasov equation for each species (1) together with the Maxwell equations (3)–(6) and the constitutive equations (7)–(10) form a closed, coupled system of non-linear partial differential equations and integral equations.

2.1. The Fourier transformed Vlasov equation

By using the Fourier transform pair,

$$f_\alpha(\mathbf{x}, \mathbf{v}, t) = \int_{-\infty}^{\infty} \widehat{f}_\alpha(\mathbf{x}, \boldsymbol{\eta}, t) \mathrm{e}^{-\mathrm{i}\boldsymbol{\eta}\cdot\mathbf{v}}\, \mathrm{d}^3 \eta, \tag{11}$$

$$\widehat{f}_\alpha(\mathbf{x}, \boldsymbol{\eta}, t) = \frac{1}{(2\pi)^3} \int_{-\infty}^{\infty} f_\alpha(\mathbf{x}, \mathbf{v}, t) \mathrm{e}^{\mathrm{i}\boldsymbol{\eta}\cdot\mathbf{v}}\, \mathrm{d}^3 v, \tag{12}$$

the velocity variable $\mathbf{v}$ is transformed into a new variable $\boldsymbol{\eta}$ and the distribution function $f(\mathbf{x}, \mathbf{v}, t)$ is changed to a new, complex valued, function $\widehat{f}(\mathbf{x}, \boldsymbol{\eta}, t)$, which obeys the transformed Vlasov equation

$$\frac{\partial \widehat{f}_\alpha}{\partial t} - \mathrm{i}\nabla_{\mathbf{x}} \cdot \nabla_{\boldsymbol{\eta}} \widehat{f}_\alpha - \frac{q_\alpha}{m_\alpha} \left(\mathrm{i}\mathbf{E} \cdot \boldsymbol{\eta} \widehat{f}_\alpha + \nabla_{\boldsymbol{\eta}} \cdot \left\{ [(\mathbf{B} + \mathbf{B}_{\mathrm{ext}}) \times \boldsymbol{\eta}] \widehat{f}_\alpha \right\} \right) = 0, \tag{13}$$

where the nabla operator $\nabla_{\boldsymbol{\eta}}$ denotes differentiation with respect to $\boldsymbol{\eta}$.

Eq. (13) together with the Maxwell equations (3)–(6) and the constitutive equations (7) and (8) where the particle number densities and mean velocities are obtained as

$$n_\alpha(\mathbf{x}, t) = (2\pi)^3 [\widehat{f}_\alpha(\mathbf{x}, \boldsymbol{\eta}, t)]_{\boldsymbol{\eta}=\mathbf{0}} = (2\pi)^3 \Re[\widehat{f}_\alpha(\mathbf{x}, \boldsymbol{\eta}, t)]_{\boldsymbol{\eta}=\mathbf{0}} \tag{14}$$

and

$$\mathbf{v}_\alpha(\mathbf{x}, t) = -\mathrm{i} \frac{(2\pi)^3}{n_\alpha(\mathbf{x}, t)} \left[\nabla_\eta \widehat{f}_\alpha(\mathbf{x}, \boldsymbol{\eta}, t) \right]_{\boldsymbol{\eta}=\mathbf{0}} = \frac{(2\pi)^3}{n_\alpha(\mathbf{x}, t)} \left\{ \nabla_\eta \Im[\widehat{f}_\alpha(\mathbf{x}, \boldsymbol{\eta}, t)] \right\}_{\boldsymbol{\eta}=\mathbf{0}}, \tag{15}$$

respectively, form a new closed set of equations. One can note that the integrals over infinite $\mathbf{v}$ space in Eqs. (9) and (10) have been converted to evaluations in $\boldsymbol{\eta}$ space in Eqs. (14) and (15). The symbols $\Re[\widehat{f}_\alpha]$ and $\Im[\widehat{f}_\alpha]$ denote respectively the real and imaginary parts of the distribution function $\widehat{f}_\alpha$. The last equalities in

Eqs. (14) and (15) follow from that the real part of the distribution function is an even function with respect to $\boldsymbol{\eta}$, while the imaginary part is an odd function with respect to $\boldsymbol{\eta}$, which follows from Eq. (12) because $f_\alpha(\mathbf{x},\mathbf{v},t)$ is real valued. For the gradient $\nabla_{\boldsymbol{\eta}}\widehat{f}_\alpha$, the real and imaginary parts are, respectively, odd and even functions with respect to $\boldsymbol{\eta}$. The constant $(2\pi)^3$ used in Eqs. (12), (14) and (15) is valid for three velocity dimensions. For n velocity dimensions the corresponding constant has the value $(2\pi)^n$.

2.2. A motivation for using the Fourier transform technique

A well-known property of the Vlasov equation is that an initially smooth solution to the equation may become oscillatory in phase space (x,v) due to *kinetic effects* as time increases, making the numerical solution of the Vlasov equation a challenging task. The velocity derivatives becomes increasingly difficult to perform numerically, with a catastrophic increase of truncation errors. The solution eventually becomes so oscillatory that it is impossible to represent on a fixed numerical grid [10,11] due to the violation of the sampling (Nyqvist) theorem, which states that more than two sampling points per "wavelength" are needed to represent the solution on a grid.

In many physical problems, the distribution of particles in velocity space is significantly non-zero in a relatively small part of velocity space, and decreases like a Gaussian function, i.e., as a Maxwellian distribution, for large values on velocity v. Mathematically, this implies that the Vlasov equation in the Fourier transformed space has a smooth solution. In order to illustrate the idea, we study the one-dimensional Vlasov equation

$$\frac{\partial f}{\partial t}+v\frac{\partial f}{\partial x}-\frac{eE}{m_e}\frac{\partial f}{\partial v}=0, \tag{16}$$

$$\frac{\partial E}{\partial x}=\frac{e}{\varepsilon_0}\left[n_0-\int_{-\infty}^{\infty}f(x,v,t)\,\mathrm{d}v\right], \tag{17}$$

and the Fourier transformed Vlasov equation

$$\frac{\partial\widehat{f}}{\partial t}-\mathrm{i}\frac{\partial^2\widehat{f}}{\partial x\,\partial\eta}+\mathrm{i}\frac{eE}{m}\eta\widehat{f}=0, \tag{18}$$

$$\frac{\partial E(x,t)}{\partial x}=\frac{e}{\varepsilon_0}\left[n_0-2\pi\widehat{f}(x,\eta,t)_{\eta=0}\right], \tag{19}$$

which are related by the Fourier transform pair

$$f(x,v,t)=\int_{-\infty}^{\infty}\widehat{f}(x,\eta,t)\mathrm{e}^{-\mathrm{i}\eta v}\,\mathrm{d}\eta, \tag{20}$$

$$\widehat{f}(x,\eta,t)=\frac{1}{2\pi}\int_{-\infty}^{\infty}f(x,v,t)\mathrm{e}^{\mathrm{i}\eta v}\,\mathrm{d}v. \tag{21}$$

If one assumes that the solution for all times vanishes as a Maxwellian for large v, with the estimate

$$|f(x,v,t)|<C\exp(-\gamma v^2) \tag{22}$$

for some positive constants C and γ, then the η derivatives of the Fourier transformed solution are bounded as

$$\left|\frac{\partial^n}{\partial\eta^n}\widehat{f}(x,\eta,t)\right| = [\text{Use Eq. (21)}] = \left|\frac{1}{2\pi}\int_{-\infty}^{\infty}(\mathrm{i}v)^n \mathrm{e}^{\mathrm{i}\eta v} f(x,v,t)\,\mathrm{d}v\right| < [\text{Use the triangle inequality}]$$
$$< \frac{1}{2\pi}\int_{-\infty}^{\infty}|(\mathrm{i}v)^n \mathrm{e}^{\mathrm{i}\eta v} f(x,v,t)|\,\mathrm{d}v = \frac{1}{2\pi}\int_{-\infty}^{\infty}|v|^n |f(x,v,t)|\,\mathrm{d}v < [\text{By (22)}]$$
$$< \frac{1}{2\pi}\int_{-\infty}^{\infty}|v|^n C\exp(-\gamma v^2)\,\mathrm{d}v = \frac{1}{2\pi}\frac{C}{\gamma^{(n+1)/2}}a_n, \tag{23}$$

where the constant

$$a_n = \begin{cases} \sqrt{\pi}2^{-n/2}(n-1)!!, & n \text{ even}, \\ [(n-1)/2]!, & n \text{ odd}, \end{cases} \tag{24}$$

and where symbols ! for the factorial and !! for the semi-factorial have their usual meaning. Thus, by the assumption (22) for $f(x,v,t)$ it follows that $\widehat{f}(x,\eta,t)$ is infinitely differentiable with respect to η with the estimate (23) for the derivatives. It is now possible to make an error estimate of the truncation error of a difference scheme used to approximate the η derivative in Eq. (18). The compact Padé scheme [20], which is used to perform numerical approximations of the first derivatives in $\boldsymbol{\eta}$ space (see [10,11]) has a truncation error of size

$$|\varepsilon| \leqslant \frac{1}{120}\Delta\eta^4 \max\left|\frac{\partial^5\widehat{f}}{\partial\eta^5}\right|, \tag{25}$$

where the fifth derivative gives $n = 5$ in the relations (23) and (24), yielding the estimate

$$|\varepsilon| < \frac{1}{2\pi}\frac{\Delta\eta^4}{60}\frac{C}{\gamma^3} \tag{26}$$

for the truncation error. It is thus possible to make an error estimate for the numerical differentiation in the Fourier transformed velocity η space in Eq. (18), which is not possible for a numerical differentiation in the original velocity v space in Eq. (16).

3. Electromagnetic waves

In the present section, the fully electromagnetic Maxwell equations are investigated. Ions and electrons are allowed to move in the plasma, giving rise to two Vlasov equations, one for ions and one for electrons.

3.1. Conserved quantities of the Vlasov–Maxwell system

The Vlasov–Maxwell system has several time-conserved quantities, of which a few of the most important conserved quantities are the energy norm

$$\|f_\alpha\|^2 = \int_{\Omega_\mathbf{x}}\int_{\Omega_\mathbf{v}} f_\alpha^2\,\mathrm{d}\Omega_\mathbf{v}\,\mathrm{d}\Omega_\mathbf{x}, \tag{27}$$

where $\Omega_\mathbf{x}$ and $\Omega_\mathbf{v}$ denote all $\mathbf{x}$ space and all velocity $\mathbf{v}$ space, respectively, and where α equals i for ions and e for electrons. The total number of particles

$$N_\alpha = \int_{\Omega_\mathbf{x}}\int_{\Omega_\mathbf{v}} f_\alpha\,\mathrm{d}\Omega_\mathbf{v}\,\mathrm{d}\Omega_\mathbf{x}, \tag{28}$$

and, if the external magnetic field $\mathbf{B}_{\text{ext}}$ is constant, then the total linear momentum, including the electromagnetic contributions [30],

$$\mathbf{p} = \int_{\Omega_{\mathbf{x}}} \left[\int_{\Omega_{\mathbf{v}}} \mathbf{v}(m_{\text{i}} f_{\text{i}} + m_{\text{e}} f_{\text{e}}) \, \mathrm{d}\Omega_{\mathbf{v}} + \varepsilon_0 \mathbf{E} \times (\mathbf{B} + \mathbf{B}_{\text{ext}}) \right] \mathrm{d}\Omega_{\mathbf{x}}, \tag{29}$$

and the total energy

$$W = \int_{\Omega_{\mathbf{x}}} \left[\int_{\Omega_{\mathbf{v}}} \frac{1}{2} v^2 (m_{\text{i}} f_{\text{i}} + m_{\text{e}} f_{\text{e}}) \, \mathrm{d}\Omega_{\mathbf{v}} + \frac{1}{2} \left(\varepsilon_0 E^2 + \frac{(\mathbf{B} + \mathbf{B}_{\text{ext}})^2}{\mu_0} \right) \right] \mathrm{d}\Omega_{\mathbf{x}} \tag{30}$$

are conserved, where $v^2 = \mathbf{v} \cdot \mathbf{v}$, $E^2 = \mathbf{E} \cdot \mathbf{E}$ and $(\mathbf{B} + \mathbf{B}_{\text{ext}})^2 = (\mathbf{B} + \mathbf{B}_{\text{ext}}) \cdot (\mathbf{B} + \mathbf{B}_{\text{ext}})$.

We note that the norm $\|f_\alpha\|$ has its counterpart in the Fourier transformed velocity space via the Parseval relation, and the other integrals also have their counterparts in the Fourier transformed space via basic properties of the Fourier transform. The corresponding expressions for the the above invariants are

$$\|\widehat{f}_\alpha\|^2 = \frac{1}{(2\pi)^n} \int_{\Omega_{\mathbf{x}}} \int_{\Omega_{\boldsymbol{\eta}}} |\, \widehat{f}_\alpha \,|^2 \, \mathrm{d}\Omega_{\boldsymbol{\eta}} \, \mathrm{d}\Omega_{\mathbf{x}}, \tag{31}$$

where $\Omega_{\boldsymbol{\eta}}$ denotes all $\boldsymbol{\eta}$ space and n is the number of velocity dimensions, and

$$N_\alpha = \int_{\Omega_{\mathbf{x}}} (2\pi)^n (\widehat{f}_\alpha)_{\boldsymbol{\eta}=\mathbf{0}} \, \mathrm{d}\Omega_{\mathbf{x}}, \tag{32}$$

$$\mathbf{p} = \int_{\Omega_{\mathbf{x}}} [-\mathrm{i}(2\pi)^n \nabla_{\boldsymbol{\eta}} (m_{\text{i}} \widehat{f}_{\text{i}} + m_{\text{e}} \widehat{f}_{\text{e}})_{\boldsymbol{\eta}=\mathbf{0}} + \varepsilon_0 \mathbf{E} \times (\mathbf{B} + \mathbf{B}_{\text{ext}})] \, \mathrm{d}\Omega_{\mathbf{x}}, \tag{33}$$

$$W = \int_{\Omega_{\mathbf{x}}} \left[-\frac{1}{2} (2\pi)^n \nabla_\eta^2 (m_{\text{i}} \widehat{f}_{\text{i}} + m_{\text{e}} \widehat{f}_{\text{e}})_{\boldsymbol{\eta}=\mathbf{0}} + \frac{1}{2} \left(\varepsilon_0 E^2 + \frac{(\mathbf{B} + \mathbf{B}_{\text{ext}})^2}{\mu_0} \right) \right] \mathrm{d}\Omega_{\mathbf{x}}, \tag{34}$$

respectively, where $\nabla_\eta^2 = \nabla_{\boldsymbol{\eta}} \cdot \nabla_{\boldsymbol{\eta}}$ is the Laplacian in $\boldsymbol{\eta}$ space. In the absence of analytical "calibration" solutions for non-linear problems, these conserved quantities are indispensable for checking the correctness of any numerical scheme used the solve the Vlasov–Maxwell system; see Section 4.4 below. Similar as in [11] for the Vlasov–Poisson system, the present problem is restricted to a bounded domain in $\boldsymbol{\eta}$ space, and outflow boundary conditions are devised in $\boldsymbol{\eta}$ space so that the norm $\|\widehat{f}_\alpha\|^2$ is a non-increasing, positive function of time, assessing that the problem is *well-posed* [15,26]. The well-posedness carries over trivially to the present Vlasov–Maxwell system, since the only difference is how to calculate the electric and magnetic fields. We point out that the discretized version of this norm is a very good indicator on whether or not a numerical scheme used is stable [10,11].

3.2. The conserved divergences of the electromagnetic field

A property of the Maxwell equations is that the two first Eqs. (3) and (4) can be seen on as parts of the *initial conditions* to the last two Eqs. (5) and (6), and also as *conserved quantities* of the Maxwell equations. The reason for this property of the Maxwell equations is that the electric charge and current densities fulfill the *continuity equation*

$$\frac{\partial \rho}{\partial t} + \nabla_{\mathbf{x}} \cdot \mathbf{j} = 0, \tag{35}$$

which historically was used by Maxwell to derive the Maxwell equations in its current form.

In a numerical solution, truncation errors are introduced in the integration of the electromagnetic fields in Eqs. (5) and (6) and in the integration of the Vlasov equation so that Eq. (35) may not be fulfilled locally. The integration of Eqs. (5) and (6) may give rise to an accumulation of errors in Eqs. (3) and (4) over time. If the divergences (3) and (4) after some time are not fulfilled, then the numerical scheme produces unphysical values for the fields, and the value of the obtained solution is questionable.

3.3. Physical and unphysical solutions

It may be appropriate here to discuss shortly what is meant by a "physical solution" of the Maxwell equations. If the two vector-valued Maxwell equations (5) and (6) are integrated numerically in time, with initial conditions which do not fulfill the divergence equations (3) and (4), then the fields are from the very beginning unphysical, and any results from the numerical simulation must be regarded as questionable. If solved together with the Vlasov equation, the unphysical fields enter as forces into the Vlasov equation where particles will be accelerated in an unphysical manner.

If, on the other hand, the divergence equations (3) and (4) *are* fulfilled at all times, up to the local truncation error of the numerical scheme, then the solution will at any time work as a physical initial condition for later times, so that *locally in time* (i.e., for short periods of time after the initial condition) one will have a solution which simulates the mathematical model up to the truncation error of the numerical scheme.

In long-time simulations, any numerical scheme will give rise to truncation errors so that the solution may deviate strongly from the exact solution, after a long time. In some situations, this may not be a problem as long as the numerical solution *behaves like* the physical system locally in time. One such example is turbulence simulations, where it is in principle impossible to follow a solution exactly for a long time, due to positive *Liapunov exponents* [27] which increase small perturbations exponentially with time. Long-time turbulence simulations may still be of value if the numerical solution behaves like the physical system to be simulated (for example: like *plasma*, or like *electromagnetic fields*) locally in time.

In this view, it is more severe if a numerical solution of the Maxwell equations does not conserve the divergences (3) and (4) after some time, because after this time the numerical solution does not resemble the behaviour of electromagnetic fields even locally in time. If the divergences *are* conserved, then the numerical solution does resemble electromagnetic fields locally in time, even if the numerical solution deviates from the exact solution.

3.4. The Lorentz inhomogeneous wave equations

An alternative description [16,28] of the fields is given by the electrodynamic *potential* and *vector potential* which are related to the electromagnetic field as

$$\mathbf{E} = -\nabla\Phi - \frac{\partial \mathbf{A}}{\partial t}, \tag{36}$$

$$\mathbf{B} = \nabla_{\mathbf{x}} \times \mathbf{A} \tag{37}$$

and which, by choosing the *Lorentz condition* for the divergence of the vector potential,

$$\nabla_{\mathbf{x}} \cdot \mathbf{A} + \frac{1}{c^2}\frac{\partial \Phi}{\partial t} = 0 \tag{38}$$

yields the *Lorentz wave equations*

$$\frac{1}{c^2}\frac{\partial^2 \Phi}{\partial t^2} - \nabla^2 \Phi = \frac{\rho}{\varepsilon_0}, \tag{39}$$

$$\frac{1}{c^2}\frac{\partial^2 \mathbf{A}}{\partial t^2} - \nabla^2 \mathbf{A} = \mu_0 \mathbf{j}. \tag{40}$$

The Lorentz wave equations is a description of the physics equivalent to the Maxwell equations (3)–(6).

In this description, the divergence of the magnetic field is zero, since the divergence of the right-hand side of Eq. (37) is zero by the vector relation $\nabla_{\mathbf{x}} \cdot (\nabla_{\mathbf{x}} \times \mathbf{A}) = 0$. The divergence of the electric field can be set to the correct value by using the Maxwell equation for the divergence of the electric field (3) together with Eq. (36), yielding

$$\nabla_{\mathbf{x}} \cdot \mathbf{E} = -\nabla^2 \Phi - \nabla_{\mathbf{x}} \cdot \frac{\partial \mathbf{A}}{\partial t} = \frac{\rho}{\varepsilon_0} \tag{41}$$

or

$$-\nabla^2 \Phi = \frac{\rho}{\varepsilon_0} + \nabla_{\mathbf{x}} \cdot \frac{\partial \mathbf{A}}{\partial t}. \tag{42}$$

This equation for Φ conserves the divergence of the electric field, and is solved [instead of Eq. (39)] together with Eq. (40).

There is a close relationship between the Lorentz condition and the continuity equation. Solving for $\mathbf{j}$ and ρ in Eqs. (40) and (42), and inserting the results into the left-hand side of the continuity equation (35), we have

$$\begin{aligned}\frac{\partial \rho}{\partial t} + \nabla_{\mathbf{x}} \cdot \mathbf{j} &= \frac{\partial}{\partial t}\left[\varepsilon_0\left(-\nabla^2 \Phi - \nabla_{\mathbf{x}} \cdot \frac{\partial \mathbf{A}}{\partial t}\right)\right] + \nabla_{\mathbf{x}} \cdot \left[\frac{1}{\mu_0}\left(\frac{1}{c^2}\frac{\partial^2 \mathbf{A}}{\partial t^2} - \nabla^2 \mathbf{A}\right)\right] \\ &= -\frac{1}{\mu_0}\nabla^2\left(\nabla_{\mathbf{x}} \cdot \mathbf{A} + \frac{1}{c^2}\frac{\partial \Phi}{\partial t}\right).\end{aligned} \tag{43}$$

If the continuity equation (35) is fulfilled exactly, leading to that the left-hand side in Eq. (43) equals zero, then it follows from the integration of the *elliptic* equation (43), with periodic boundary conditions (which we will have in the present article), that the Lorentz condition (38) is fulfilled. This is shown by a Fourier decomposition of the potentials,

$$\Phi(\mathbf{x}, t) = \sum_{\mathbf{k}} \widehat{\Phi}_{\mathbf{k}}(t) \exp[\mathrm{i}(\mathbf{k} \cdot \mathbf{x})], \tag{44}$$

$$\mathbf{A}(\mathbf{x}, t) = \sum_{\mathbf{k}} \widehat{\mathbf{A}}_{\mathbf{k}}(t) \exp[\mathrm{i}(\mathbf{k} \cdot \mathbf{x})], \tag{45}$$

which inserted into Eq. (43) (with the left-hand side equal to zero) leads to that the Fourier components of $\mathbf{A}$ and Φ for $k^2 \neq 0$ fulfill the Fourier transformed Lorentz condition since

$$0 = \frac{k^2}{\mu_0}\left(\mathrm{i}\mathbf{k} \cdot \mathbf{A}_{\mathbf{k}} + \frac{1}{c^2}\frac{\partial \Phi_{\mathbf{k}}}{\partial t}\right) \tag{46}$$

or

$$\left(\mathrm{i}\mathbf{k} \cdot \mathbf{A}_{\mathbf{k}} + \frac{1}{c^2}\frac{\partial \Phi_{\mathbf{k}}}{\partial t}\right) = 0, \quad k^2 \neq 0. \tag{47}$$

If the Fourier component of Φ corresponding to $k^2 = 0$ is set to zero, $\widehat{\Phi}_{\mathbf{0}}(t) = 0$, in the numerical solution of Eq. (42), then each Fourier component $\mathbf{A}_{\mathbf{k}}$ and $\Phi_{\mathbf{k}}$ fulfills the Lorentz condition and which therefore also $\mathbf{A}$ and Φ do. As a contrast, if Eq. (39) [instead of Eq. (42)] is solved together with Eq. (40), then the Lorentz condition is not necessarily fulfilled: Solving ρ and $\mathbf{j}$ Eqs. (39) and (40), and inserting the results into the left-hand side of the continuity equation (35) gives

$$\frac{\partial \rho}{\partial t} + \nabla_{\mathbf{x}} \cdot \mathbf{j} = \frac{1}{\mu_0}\left(\frac{1}{c^2}\frac{\partial^2}{\partial t^2} - \nabla^2\right)\left(\nabla_{\mathbf{x}} \cdot \mathbf{A} + \frac{1}{c^2}\frac{\partial \Phi}{\partial t}\right). \tag{48}$$

If the continuity equation (35) is again fulfilled exactly, leading to that the left-hand side in Eq. (48) equals zero, then the integration of this *hyperbolic* equation, with periodic boundary conditions, will give that the Lorentz condition (38) is only fulfilled if also the *initial conditions* of Eq. (48) are specified correctly. Therefore the system (40) and (42) is more "robust" in the sense that the Lorentz condition will be satisfied at all times regardless on the initial condition on $\mathbf{A}$, if the continuity equation is fulfilled exactly. This somewhat surprising result comes from that in the solution of (40) and (42), one only has to specify initial conditions on $\mathbf{A}$ (and not on Φ) leading to that the Lorentz condition is fulfilled, while in the solution of Eqs. (39) and (40) one has to specify initial conditions on both $\mathbf{A}$ and Φ; it is then easy to specify initial conditions on the time derivative of Φ so that the Lorentz condition is violated.

If the continuity equation is *not* fulfilled exactly in the numerical solution of the Vlasov equation, then the Lorentz condition will also be violated, which follows from Eqs. (43) and (48). A nice property of Eq. (43) [which was derived from Eqs. (40) and (42)] is that the violation of the Lorenz condition is local in time and the errors therefore not will accumulate over time. On the other hand, if the system (39), (40) is solved, then any error in the continuity equation will act as a source to the hyperbolic equation (48) and errors may accumulate over time in the Lorentz condition, making the solution increasingly incompatible with the Maxwell equations. Apparently, the system (40) and (42) is more robust than the system (39) and (40) if errors are introduced in the continuity equation.

Finally we discuss the relationship between Eqs. (39) and (42): Solving for ρ in Eq. (39) and inserting the result into Eq. (42) gives the result

$$\frac{\partial}{\partial t}\left(\nabla_{\mathbf{x}} \cdot \mathbf{A} + \frac{1}{c^2}\frac{\partial \Phi}{\partial t}\right) = 0, \tag{49}$$

which is fulfilled if the Lorentz condition is fulfilled. We have shown that the Lorentz condition is fulfilled (if the continuity condition is fulfilled), in the solution of the system (40) and (42), and we therefore conclude that every solution of the system (40) and (42) gives solutions Φ and $\mathbf{A}$ which are solutions to Eqs. (39) and (40). The opposite does not hold, since in the system (39) and (40) it is possible to give initial conditions which violate the Lorentz condition and therefore the system (39) and (40) can produce solutions which are not necessarily solutions to the system (40) and (42).

By introducing a separate variable $\mathbf{\Gamma}$ for the time derivative of the vector potential $\mathbf{A}$, the Lorentz wave equations (40) and (42) can be rewritten in a first-order system with respect to time,

$$\frac{\partial \mathbf{A}}{\partial t} = \mathbf{\Gamma}, \quad \frac{\partial \mathbf{\Gamma}}{\partial t} = c^2(\nabla^2 \mathbf{A} + \mu_0 \mathbf{j}), \tag{50}$$

$$-\nabla^2 \Phi = \frac{\rho}{\varepsilon_0} + \nabla_{\mathbf{x}} \cdot \mathbf{\Gamma}, \tag{51}$$

and the electric and magnetic fields are calculated as

$$\mathbf{E} = -\nabla \Phi - \mathbf{\Gamma} \tag{52}$$

and

$$\mathbf{B} = \nabla_{\mathbf{x}} \times \mathbf{A}, \tag{53}$$

respectively, in the new variables.

The system (50)–(53) produces physical electric and magnetic fields *regardless of the initial conditions on* $\mathbf{A}$ *and* $\mathbf{\Gamma}$, in the sense that the first two Maxwell equations for the divergences (3) and (4) are fulfilled. Therefore, a consistent numerical scheme will also produce physical solutions, up to the local truncation error of the numerical scheme, even after a long time; no artificial electric and magnetic charges are created and accumulated by the numerical scheme, which could be the case if the two last Maxwell equations (5) and (6) are integrated numerically in time. This general property of the system is an advantage, since it is not necessary to use special, divergence-conserving schemes to solve these equations, and it therefore opens up the possibility to switch between different numerical methods without having to pay too much attention to the divergences of the electromagnetic field. In complicated geometries, it may be a disadvantage that an elliptic equation (51) has to be solved numerically to obtain the potential Φ. In our case, however, the geometry is very simple and there are no problems to solve this elliptic equation efficiently by means of Fourier transform techniques.

4. The scaled, two-dimensional Vlasov–Maxwell system

We restrict the Vlasov–Maxwell system to two spatial and two velocity dimensions. We consider an external and a self-consistent magnetic field $\mathbf{B}_{\text{ext}} = \widehat{\mathbf{x}}_3 B_{\text{ext}}$ and $\mathbf{B}(x_1, x_2, t) = \widehat{\mathbf{x}}_3 B(x_1, x_2, t)$, respectively, where $\widehat{\mathbf{x}}_3$ is the unit vector along the magnetic field lines. The electric field $\mathbf{E}$, the current density $\mathbf{j}$ and the potentials $\mathbf{A}$ and $\mathbf{\Gamma}$ are directed in the plane perpendicular to the magnetic field lines, i.e., the electric field is $\mathbf{E}(x_1, x_2, t) = \widehat{\mathbf{x}}_1 E_1(x_1, x_2, t) + \widehat{\mathbf{x}}_2 E_2(x_1, x_2, t)$, where $\widehat{\mathbf{x}}_1$ and $\widehat{\mathbf{x}}_2$ are the Cartesian unit vectors in the x_1 and x_2 directions, respectively, and similarly for $\mathbf{j}$, $\mathbf{A}$ and $\mathbf{\Gamma}$. The dynamics of the system in velocity space and the Fourier velocity space is restricted to the plane perpendicular to the magnetic field, i.e., $\mathbf{v} = \widehat{\mathbf{x}}_1 v_1 + \widehat{\mathbf{x}}_2 v_2$ and $\boldsymbol{\eta} = \widehat{\mathbf{x}}_1 \eta_1 + \widehat{\mathbf{x}}_2 \eta_2$. We use the scaling of variables according to Eqs. (16)–(18) in [11], plus a scaling of the vector potentials, charge and current densities, and ion distribution functions into dimensionless, primed quantities as

$$t = \omega_{\text{pe}}^{-1} t', \tag{54}$$

$$v_1 = v_{\text{th,e}} v_1', \quad v_2 = v_{\text{th,e}} v_2', \tag{55}$$

$$x_1 = r_{\text{D}} x_1', \quad x_2 = r_{\text{D}} x_2', \tag{56}$$

$$\eta_1 = v_{\text{th,e}}^{-1} \eta_1', \quad \eta_2 = v_{\text{th,e}}^{-1} \eta_2', \tag{57}$$

$$\widehat{f}_{\text{e}} = n_0 \widehat{f}_{\text{e}}', \quad \widehat{f}_{\text{i}} = n_0 \widehat{f}_{\text{i}}', \tag{58}$$

$$f_{\text{e}} = n_0 v_{\text{th,e}}^{-2} f_{\text{e}}', \quad f_{\text{i}} = n_0 v_{\text{th,e}}^{-2} f_{\text{i}}', \tag{59}$$

$$E_1 = v_{\text{th,e}}^2 r_{\text{D}}^{-1} (m_{\text{e}}/e) E_1', \quad E_2 = v_{\text{th,e}}^2 r_{\text{D}}^{-1} (m_{\text{e}}/e) E_2', \tag{60}$$

$$\Phi = v_{\text{th,e}}^2 (m_{\text{e}}/e) \Phi', \tag{61}$$

$$B_{\text{ext}} = \omega_{\text{pe}}(m_{\text{e}}/e)B'_{\text{ext}}, \quad B = \omega_{\text{pe}}(m_{\text{e}}/e)B', \tag{62}$$

$$A_1 = v_{\text{th,e}}\frac{m_{\text{e}}}{e}A'_1, \quad A_2 = v_{\text{th,e}}\frac{m_{\text{e}}}{e}A'_2, \tag{63}$$

$$\Gamma_1 = \omega_{\text{pe}}v_{\text{th,e}}\frac{m_{\text{e}}}{e}\Gamma'_1, \quad \Gamma_2 = \omega_{\text{pe}}v_{\text{th,e}}\frac{m_{\text{e}}}{e}\Gamma'_2, \tag{64}$$

$$\rho = n_0 e\rho', \tag{65}$$

$$j_1 = v_{\text{th,e}}n_0 e j'_1, \quad j_2 = v_{\text{th,e}}n_0 e j'_2, \tag{66}$$

where n_0 is the *background electron particle number density*, $\omega_{\text{pe}} = \sqrt{n_0e^2/\varepsilon_0 m_{\text{e}}}$ is the *electron plasma frequency*, $v_{\text{th,e}} = \sqrt{k_{\text{B}}T_{\text{e}}/m_{\text{e}}}$ is the is the *electron thermal velocity*, k_{B} is *Boltzmann's constant*, T_{e} is the *electron temperature* and $r_{\text{D}} = v_{\text{th,e}}/\omega_{\text{pe}}$ is the *electron Debye length*. With this scaling, the Fourier transformed Vlasov equation for the ions and electrons attain the dimensionless form, omitting the primes,

$$\frac{\partial\widehat{f}_{\text{i}}}{\partial t} - \text{i}\frac{\partial^2\widehat{f}_{\text{i}}}{\partial x_1\partial\eta_1} - \text{i}\frac{\partial^2\widehat{f}_{\text{i}}}{\partial x_2\partial\eta_2} - \frac{m_{\text{e}}}{m_{\text{i}}}\left[\text{i}(E_1\eta_1 + E_2\eta_2)\widehat{f}_{\text{i}} + (B_{\text{ext}} + B)\left(\eta_1\frac{\partial\widehat{f}_{\text{i}}}{\partial\eta_2} - \eta_2\frac{\partial\widehat{f}_{\text{i}}}{\partial\eta_1}\right)\right] = 0, \tag{67}$$

$$\frac{\partial\widehat{f}_{\text{e}}}{\partial t} - \text{i}\frac{\partial^2\widehat{f}_{\text{e}}}{\partial x_1\partial\eta_1} - \text{i}\frac{\partial^2\widehat{f}_{\text{e}}}{\partial x_2\partial\eta_2} + \left[\text{i}(E_1\eta_1 + E_2\eta_2)\widehat{f}_{\text{e}} + (B_{\text{ext}} + B)\left(\eta_1\frac{\partial\widehat{f}_{\text{e}}}{\partial\eta_2} - \eta_2\frac{\partial\widehat{f}_{\text{e}}}{\partial\eta_1}\right)\right] = 0, \tag{68}$$

respectively. The Lorentz wave equations (39) and (40) attain the dimensionless form

$$\frac{\partial^2\Phi}{\partial t^2} - \left(\frac{c}{v_{\text{th,e}}}\right)^2\nabla^2\Phi = \left(\frac{c}{v_{\text{th,e}}}\right)^2\rho, \tag{69}$$

$$\frac{\partial^2\mathbf{A}}{\partial t^2} - \left(\frac{c}{v_{\text{th,e}}}\right)^2\nabla^2\mathbf{A} = \mathbf{j}, \tag{70}$$

and the first-order system (50) and (51) takes the form

$$\frac{\partial A_1}{\partial t} = \Gamma_1, \quad \frac{\partial\Gamma_1}{\partial t} = \left(\frac{c}{v_{\text{th,e}}}\right)^2\left(\frac{\partial^2A_1}{\partial x_1^2} + \frac{\partial^2A_1}{\partial x_2^2}\right) + j_1, \tag{71}$$

$$\frac{\partial A_2}{\partial t} = \Gamma_2, \quad \frac{\partial\Gamma_2}{\partial t} = \left(\frac{c}{v_{\text{th,e}}}\right)^2\left(\frac{\partial^2A_2}{\partial x_1^2} + \frac{\partial^2A_2}{\partial x_2^2}\right) + j_2, \tag{72}$$

$$-\left(\frac{\partial^2\Phi}{\partial x_1^2} + \frac{\partial^2\Phi}{\partial x_2^2}\right) = \rho + \frac{\partial\Gamma_1}{\partial x_1} + \frac{\partial\Gamma_2}{\partial x_2}, \tag{73}$$

and the dimensionless electric and magnetic fields are calculated as

$$E_1 = -\frac{\partial\Phi}{\partial x_1} - \Gamma_1, \quad E_2 = -\frac{\partial\Phi}{\partial x_2} - \Gamma_2, \tag{74}$$

and

$$B = \frac{\partial A_2}{\partial x_1} - \frac{\partial A_1}{\partial x_2}, \tag{75}$$

respectively. The charge and current densities are calculated from the ion and electron distribution functions [cf. Eqs. (14) and (15)] as

$$\rho = (2\pi)^2 [\Re(\widehat{f}_\mathrm{i}) - \Re(\widehat{f}_\mathrm{e})]_{\eta_1=\eta_2=0}, \tag{76}$$

$$j_1 = (2\pi)^2 \left[\frac{\partial \Im(\widehat{f}_\mathrm{i})}{\partial \eta_1} - \frac{\partial \Im(\widehat{f}_\mathrm{e})}{\partial \eta_1} \right]_{\eta_1=\eta_2=0}, \tag{77}$$

$$j_2 = (2\pi)^2 \left[\frac{\partial \Im(\widehat{f}_\mathrm{i})}{\partial \eta_2} - \frac{\partial \Im(\widehat{f}_\mathrm{e})}{\partial \eta_2} \right]_{\eta_1=\eta_2=0}, \tag{78}$$

respectively.

4.1. Discretisation

Similar as [11], we discretise the problem on a rectangular, equidistant grid. The known variables in $\mathbf{x}$ space are discretised as $x_{1,i_1} = i_1 \Delta x_1$ where $i_1 = 0, 1, \ldots, N_{x_1} - 1$ and $x_{2,i_2} = i_2 \Delta x_2$ where $i_2 = 0, 1, \ldots, N_{x_2} - 1$; the grid sizes are $\Delta x_1 = L_1/N_{x_1}$ and $\Delta x_2 = L_2/N_{x_2}$ where L_1 and L_2 are the domain sizes in the x_1 and x_2 directions, respectively.

In $\boldsymbol{\eta}$ space one is free to use different domain sizes for the ion and electron Fourier transformed Vlasov equations, (or, in $\mathbf{v}$ space for the original Vlasov equations). This is convenient, because one can use the most efficient discretisation in $\boldsymbol{\eta}$ (or $\mathbf{v}$) space for each particle distribution function; in many problems, ions occupy a smaller part of the velocity $\mathbf{v}$ space than the more mobile electrons, and therefore a smaller domain size can be used in $\mathbf{v}$ space, and a *larger* domain size in $\boldsymbol{\eta}$ space. Thus, we use the domain size $0 \leqslant \eta_1 \leqslant \eta_{1,\alpha,\max}$ and $-\eta_{2,\alpha,\max} \leqslant \eta_2 \leqslant \eta_{2,\alpha,\max}$ for particle species $\alpha = \mathrm{i}, \mathrm{e}$ where i and e denote ions and electrons, respectively. The known Fourier transformed velocity variables are for particle species α discretized as $\eta_{1,\alpha,j_1} = j_1 \Delta\eta_{1,\alpha}$ where $j_1 = 0, 1, \ldots, N_{\eta_1}$ and $\eta_{2,\alpha,j_2} = j_2 \Delta\eta_{2,\alpha}$ where $j_2 = -N_{\eta_2}, \ldots, -1, 0, 1, \ldots, N_{\eta_2}$. For negative $\eta_{1,\alpha}$, we use the symmetry due to the real-valued distribution functions in $\mathbf{v}$ space, described in [11]. The grid sizes are $\Delta\eta_{1,\alpha} = \eta_{1,\alpha,\max}/N_{\eta_1}$ and $\Delta\eta_{2,\alpha} = \eta_{2,\alpha,\max}/N_{\eta_2}$. The time is discretised as $t_k = t_{k-1} + \Delta t_k$ where $k = 1, 2, \ldots, N_t$, and where the time time step Δt_k is calculated adaptively; see Section 4.3 below.

The particle distribution functions for particle species α is discretized and enumerated such that $\widehat{f}_\alpha(x_{1,i_1}, x_{2,i_2}, \eta_{1,\alpha,j_1}, \eta_{2,\alpha,j_2}, t_k) \approx \widehat{f}^k_{\alpha,i_1,i_2,j_1,j_2}$. The electrodynamic potential is discretised as $\Phi(x_{1,i_1}, x_{2,i_2}, t_k) \approx \Phi^k_{i_1,i_2}$ and similarly for the quantities E_1, E_2, A_1, A_2, Γ_1 and Γ_2.

For convenience, we have used the same numbers of grid points N_{η_1} and N_{η_2} in the discretisation of $\boldsymbol{\eta}$ space for both the electron and ion Vlasov equations, and we have used even numbers of grid points N_{x_1} and N_{x_2} in the discretisation of $\mathbf{x}$ space. Note that we have used the same symbols j_1 and j_2 both to denote the current densities in Eqs. (77) and (78), and and to denote indices in the present section, but we think that the meaning of these symbols should be clear from the context.

4.2. The numerical integration of the Lorentz–Vlasov system

The Vlasov equation for ions (67) is solved with the method described in [11], where in the treatment of boundary conditions in $\boldsymbol{\eta}$ space, one has to take into account the factor $(-m_\mathrm{e}/m_\mathrm{i})$ multiplying the magnetic field. This is straightforwardly done by replacing B by $B' = (-m_\mathrm{e}/m_\mathrm{i})(B + B_\mathrm{ext})$ in [11].

The Lorentz system (71) and (72) is invoked into the Runge–Kutta time stepping scheme described in [11]. The calculation of the x_1 and x_2 derivatives in Eqs. (71)–(75), and the integration of the elliptic equation (73) for Φ is performed with pseudo-spectral methods, in a similar manner as in [11].

The $\boldsymbol{\eta}$ derivatives needed to calculate the current density $\mathbf{j}$ in Eqs. (77) and (78) are approximated by sixth-order difference schemes. For the ion and electron distribution functions ($\widehat{f}_{\mathrm{i}}$ and $\widehat{f}_{\mathrm{e}}$, denoted by $\widehat{f}_{\alpha}$), the scheme [25] for the η_1 derivative is

$$\left[\frac{\partial \Im(\widehat{f}_{\alpha})}{\partial \eta_1}\right]_{\boldsymbol{\eta}=0} \approx \frac{g_3 - 9g_2 + 45g_1 - 45g_{-1} + 9g_{-2} - g_{-3}}{60\Delta\eta_{1,\alpha}} \tag{79}$$

$$= \frac{g_3 - 9g_2 + 45g_1}{30\Delta\eta_{1,\alpha}}, \tag{80}$$

where g_{j_1} is used for $\Im(\widehat{f}_{\alpha})^{k}_{i_1,i_2,j_1,0}$ and $\Delta\eta_{1,\alpha}$ is used for $\Delta\eta_{1,\mathrm{i}}$ and $\Delta\eta_{1,\mathrm{e}}$. The last equality follows again from the symmetry property of the imaginary part of the distribution function, which is odd with respect to $\boldsymbol{\eta}$, so that $\Im(\widehat{f}_{\alpha})^{k}_{i_1,i_2,-j_1,0} = -\Im(\widehat{f}_{\alpha})_{i_1,i_2,j_1,0}$. Similarly, for the η_2 derivative,

$$\left[\frac{\partial \Im(\widehat{f}_{\alpha})}{\partial \eta_2}\right]_{\boldsymbol{\eta}=0} \approx \frac{h_3 - 9h_2 + 45g_1}{30\Delta\eta_{2,\alpha}}, \tag{81}$$

where h_{j_2} is written for $\Im(\widehat{f}_{\alpha})^{k}_{i_1,i_2,0,j_2}$ and $\Delta\eta_{2,\alpha}$ is used for $\Delta\eta_{2,\mathrm{i}}$ and $\Delta\eta_{2,\mathrm{e}}$.

4.3. Stability constraints on the time step

The analysis of the numerical stability condition on the time step size follows the analysis in Section 3.3 in [11] for the Vlasov equation for electrons. The stability condition for the solution of the homogeneous ($\mathbf{j} = \mathbf{0}$) Lorentz wave equations (71) and (72) with the Runge–Kutta method is

$$\Delta t < \frac{\sqrt{8}}{\lambda_{\max,\mathrm{L}}}, \tag{82}$$

where the largest eigenvalue is given by

$$\lambda_{\max,\mathrm{L}} = \frac{c}{v_{\mathrm{th,e}}}\sqrt{K_{x_1}^2 + K_{x_2}^2}, \tag{83}$$

where the maximum values of approximations of wave numbers by the pseudo-spectral method [11] are

$$K_{x_1} = \frac{\pi}{\Delta x_1}, \tag{84}$$

$$K_{x_2} = \frac{\pi}{\Delta x_2}. \tag{85}$$

The stability conditions for the electron and ion Vlasov equations are calculated, similarly as in Section 3.3 in [11], to be

$$\lambda_{\max,\mathrm{e}} = \frac{\pi}{\Delta x_1}\frac{\sqrt{3}}{\Delta\eta_{1,\mathrm{e}}} + \frac{\pi}{\Delta x_2}\frac{\sqrt{3}}{\Delta\eta_{2,\mathrm{e}}} + E_{1,\max}\eta_{1,\mathrm{e},\max} + E_{2,\max}\eta_{2,\mathrm{e},\max} + B_{\max}\eta_{1,\mathrm{e},\max}\frac{\sqrt{3}}{\Delta\eta_{2,\mathrm{e}}} + B_{\max}\eta_{2,\mathrm{e},\max}\frac{\sqrt{3}}{\Delta\eta_{1,\mathrm{e}}} \tag{86}$$

and

$$\lambda_{\max,\mathrm{i}} = \frac{\pi}{\Delta x_1}\frac{\sqrt{3}}{\Delta \eta_{1,\mathrm{i}}} + \frac{\pi}{\Delta x_2}\frac{\sqrt{3}}{\Delta \eta_{2,\mathrm{i}}} + \frac{m_\mathrm{e}}{m_\mathrm{i}}\left(E_{1,\max}\eta_{1,\mathrm{i},\max} + E_{2,\max}\eta_{2,\mathrm{i},\max} + B_{\max}\eta_{1,\mathrm{i},\max}\frac{\sqrt{3}}{\Delta\eta_{2,\mathrm{i}}} + B_{\max}\eta_{2,\mathrm{i},\max}\frac{\sqrt{3}}{\Delta\eta_{1,\mathrm{i}}}\right), \tag{87}$$

respectively.

The total stability condition is determined by the most restrictive one, and is given by

$$\Delta t = CFL\frac{\sqrt{8}}{\lambda_{\max}}, \tag{88}$$

where the maximum eigenvalue of the scheme is given by

$$\lambda_{\max} = \max(\lambda_{\max,\mathrm{L}}, \lambda_{\max,\mathrm{e}}, \lambda_{\max,\mathrm{i}}) \tag{89}$$

and where the positive CFL number obeys the condition

$$CFL < 1 \tag{90}$$

for stability.

Similarly to [11], the artificial boundaries at $\eta_1 = \eta_{1,\max}$ and at $\eta_2 = \pm\eta_{2,\max}$ are not included in the present analysis.

4.4. The conserved quantities

4.4.1. The number of particles

It shown in [11] that the numerical scheme conserves globally the number of particles (32) exactly, approximated by the sum representation

$$N_\alpha = (2\pi)^2 \sum_{i_1=0}^{N_{x_1}-1}\sum_{i_2=0}^{N_{x_2}-1} \widehat{f}_{\alpha,i_1,i_2,0,0}\Delta x_2 \Delta x_1 \tag{91}$$

of the integrals in (32), where $\widehat{f}$ is evaluated at $\boldsymbol{\eta} = \mathbf{0}$. This has been verified in the numerical experiments presented in this article, where the number of particles has been conserved by the numerical scheme up to the precision of the computer. It stems from that, along $\boldsymbol{\eta} = \mathbf{0}$, Eq. (13) reduces to

$$\left(\frac{\partial \widehat{f}_\alpha}{\partial t}\right)_{\boldsymbol{\eta}=\mathbf{0}} - (\mathrm{i}\nabla_\mathbf{x}\cdot\nabla_{\boldsymbol{\eta}}\widehat{f}_\alpha)_{\boldsymbol{\eta}=\mathbf{0}} = 0 \tag{92}$$

which, by the definitions of the particle number densities (9) and mean velocities (10), simply expresses the continuity equation for the particles

$$\frac{\partial n_\alpha}{\partial t} + \nabla_\mathbf{x}\cdot(n_\alpha \mathbf{v}_a) = 0. \tag{93}$$

In the numerical scheme used to approximate the Vlasov equation, the the total number of particles is fulfilled exactly, and locally up to the truncation error of the scheme, which solves the discretized version of Eq. (92).

4.4.2. The total linear momentum and energy

In order to assess that the numerical scheme conserves the total linear momentum and energy up to the accuracy of the numerical scheme, a numerical experiment was carried out for a fully non-linear problem.

We used parameters consistent with the conditions in the Earth's magnetosphere: the ion-electron mass ratio was set to $m_i/m_e = 1836$, the speed of light to electron thermal velocity ratio was set to $c/v_{th,e} = 70$, the ratio ion-electron temperature ratio was set to $T_i/T_e = 8$, and the external magnetic field was set to $B_{ext} = 0.115$. As an initial condition, we assume a neutral but non-uniform density distribution in space, with a population of the electrons moving relative to the ions and to the background electrons with the mean velocity $v_0 = 0.5$. The electron distribution function in velocity $\mathbf{v}$ space was set to

$$f_e(x_1,x_2,v_1,v_2,0) = \frac{1}{(2\pi)}\left\{\exp\left[-\frac{1}{2}(v_1^2+v_2^2)\right] + 0.5\exp\left\{-[0.01(x_1-250\pi)]^2 - [0.01(x_2-250\pi)]^2\right\}\exp\left[-\frac{1}{2}((v_1-v_0)^2+v_2^2)\right]\right\} \tag{94}$$

and the ions

$$f_i(x_1,x_2,v_1,v_2,0) = \frac{1}{(2\pi)}\left(\frac{v_{th,e}}{v_{th,i}}\right)^2\left(1+0.5\exp\left\{-[0.01(x_1-250\pi)]^2 - [0.01(x_2-250\pi)]^2\right\}\right)\exp\left[-\frac{1}{2}(v_1^2+v_2^2)\left(\frac{v_{th,e}}{v_{th,i}}\right)^2\right]. \tag{95}$$

In the Fourier transformed velocity space, these initial conditions become, for the electrons and ions, respectively,

$$\widehat{f}_e(x_1,x_2,\eta_1,\eta_2,0) = \frac{1}{(2\pi)^2}\exp\left[-\frac{1}{2}(\eta_1^2+\eta_2^2)\right]\left(1+A\exp(iv_0\eta_1)\exp\left\{-[0.01(x_1-250\pi)]^2 - [0.01(x_2-250\pi)]^2\right\}\right) \tag{96}$$

and

$$\widehat{f}_i(x_1,x_2,\eta_1,\eta_2,0) = \frac{1}{(2\pi)^2}\exp\left[-\frac{1}{2}(\eta_1^2+\eta_2^2)\left(\frac{v_{th,e}}{v_{th,i}}\right)^{-2}\right]\left(1+A\exp\left\{-[0.01(x_1-250\pi)]^2 - [0.01(x_2-250\pi)]^2\right\}\right). \tag{97}$$

We point out that the Fourier transformation of initial conditions could be performed analytically here but may be necessary to perform numerically for more complicated cases.

The parameters used in the numerical simulation in the present section are as follows: The spatial domain was set to $0 \leqslant x_1 \leqslant 500\pi$ and $0 \leqslant x_2 \leqslant 500\pi$. For the electron Vlasov equation $0 \leqslant \eta_1 \leqslant 10$ and $-10 \leqslant \eta_2 \leqslant 10$ and for the ion Vlasov equation $0 \leqslant \eta_1 \leqslant 100$ and $-200 \leqslant \eta_2 \leqslant 100$. The number of intervals was set to $N_{x_1} = 30$, $N_{x_2} = 30$, $N_{\eta_1} = 30$ and $2N_{\eta_2} = 60$. The number of time steps taken was $N_t = 2114$; the end time was $t_{end} = 417$. No numerical dissipation was used.

In the scaled variables used, the expressions for the total linear momentum (29) and energy (30) attain the form

$$\mathbf{p}_{tot} = \int_{\Omega_{\mathbf{x}}}\left[-i(2\pi)^2\nabla_{\boldsymbol{\eta}}\left(\frac{m_i}{m_e}\widehat{f}_i+\widehat{f}_e\right)_{\boldsymbol{\eta}=\mathbf{0}} + \mathbf{E}\times(\mathbf{B}+\mathbf{B}_{ext})\right]d\Omega_{\mathbf{x}} \equiv \mathbf{p}_{matter}+\mathbf{p}_{EM}, \tag{98}$$

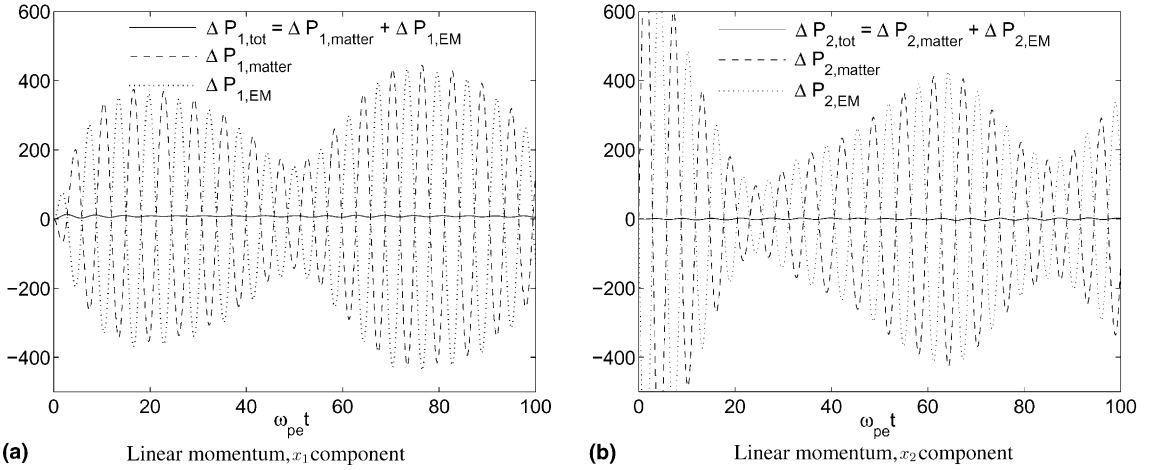

Fig. 1. The time development of x_1 and x_2 components of the total linear momentum $\Delta\mathbf{p}_{\text{tot}}$, which is the sum of the linear momentum of the matter $\Delta\mathbf{p}_{\text{matter}}$ and the linear momentum of the electromagnetic field $\Delta\mathbf{p}_{\text{EM}}$. (a) Linear momentum, x_1 component. (b) Linear momentum, x_2 component.

where $\mathbf{p}_{\text{matter}}$ and $\mathbf{p}_{\text{EM}}$ are the contribution to the linear momentum from the particles and electromagnetic field, respectively, and

$$W_{\text{tot}} = \int_{\Omega_{\mathbf{x}}} \left\{ -\frac{1}{2}(2\pi)^2 \nabla_\eta^2 \left(\frac{m_{\text{i}}}{m_{\text{e}}} \widehat{f}_{\text{i}} + \widehat{f}_{\text{e}} \right)_{\boldsymbol{\eta}=\mathbf{0}} + \frac{1}{2}\left[E^2 + \frac{c^2}{v_{\text{th,e}}^2} (\mathbf{B} + \mathbf{B}_{\text{ext}})^2 \right] \right\} \mathrm{d}\Omega_{\mathbf{x}}$$
$$\equiv W_{\text{kinetic}} + W_{\text{E}} + W_{\text{B}}, \tag{99}$$

respectively, where W_{kinetic}, W_{E} and W_{B} is the kinetic, electric and magnetic energy, respectively. The integrals are taken over the rectangular domain in (x_1, x_2) space, approximated numerically with sum representations. The gradient operator $\nabla_{\boldsymbol{\eta}} = \widehat{\mathbf{x}}_1 \partial/\partial\eta_1 + \widehat{\mathbf{x}}_2 \partial/\partial\eta_2$ and Laplace operator $\nabla_\eta^2 = \partial^2/\partial\eta_1^2 + \partial^2/\partial\eta_2^2$ are approximated numerically with sixth-order difference approximations [25].

In Fig. 1 the x_1 and x_2 components of the total linear momentum is plotted, together with the particle linear momentum and electromagnetic field linear momentum. The momentum at time zero has been subtracted (indicated by Δ) to make the comparison easier. It is clear that the total particle momentum $p_{1,\text{matter}}$, $p_{2,\text{matter}}$ and electromagnetic momentum $p_{1,\text{EM}}$, $p_{2,\text{EM}}$ perform large-amplitude fluctuations, but the total momentum $p_{1,\text{tot}}$, $p_{2,\text{tot}}$ remains almost constant with only small fluctuations. Similarly in Fig. 2, variation of the total energy W_{tot} is plotted together with the variation of the kinetic energy W_{kinetic}, the electric energy W_{E} and the magnetic energy W_{B}. Clearly, the total energy is almost constant, while the kinetic and eletromagnetic energies are fluctuating. One can see both high-frequency fluctuations performed by the electrons and also a slower development on an ion time scale where the magnetic energy is converted into kinetic energy.

4.5. Electron and ion X waves

Electromagnetic waves propagating in vacuum can have two different polarisations, with identical dispersive properties, i.e., both wave modes travel with the speed of light. With the presence of a static magnetic field in a plasma makes, this symmetry is broken and the two polarisations break into two separate wave modes, the so-called ordinary (O) and "fast" extraordinary (X) modes with different dispersive properties; see, e.g. [4] or [14] where these wave modes are discussed. Being able to travel both in

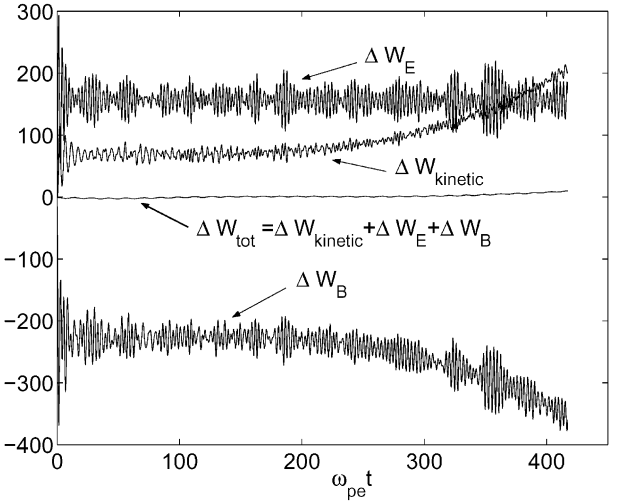

Fig. 2. The time development of the total energy ΔW_{tot}, which is the sum of the electric energy ΔW_{E}, magnetic energy ΔW_{B} and kinetic energy of the matter $\Delta W_{\text{kinetic}}$.

vacuum and plasma, X and O modes are of special interest in the studies of distant objects in the universe, since electromagnetic waves is often the only source of information from these objects. Except for these wave modes, there exist also a "slow" X mode which is also a high-frequency mode with a slightly lower frequency than the fast X mode, and a low-frequency ion X mode. We mention that these named wave modes are the ones which can be studied in a fluid (Navier–Stokes) description of the plasma. In a kinetic (Vlasov) description of the plasma, these wave modes turn out to be only a few of the infinitely many branches of Bernstein waves; see, e.g. [24] who studied the linear behavior of electromagnetic ion and electron Bernstein waves. The linear X modes and Bernstein waves will, together with a fully non-linear problem, be studied numerically in the present section.

An approximate dispersion law for the high frequency electromagnetic wave perpendicular to the magnetic field, obtained from a fluid description of cold electrons [14], is given by

$$\frac{c^2k^2}{\omega^2} = 1 - \frac{\omega_{\text{pe}}^2(\omega^2 - \omega_{\text{pe}}^2)}{\omega^2(\omega^2 - \omega_{\text{uh}}^2)}, \tag{100}$$

where $\omega_{\text{uh}} = \sqrt{\omega_{\text{pe}}^2 + \omega_{\text{ce}}^2}$ is the *upper hybrid frequency* and $\omega_{\text{ce}} = eB_{\text{ext}}/m_{\text{e}}$ is the *electron cyclotron frequency*. By using the relation $v_{\text{th,e}} = \omega_{\text{pe}} r_{\text{D}}$ in the left-hand side of Eq. (100), the equation is rewritten as

$$\frac{(c/v_{\text{th,e}})^2(kr_{\text{D}})^2(\omega_{\text{pe}}/\omega_{\text{ce}})^2}{(\omega/\omega_{\text{ce}})^2} = 1 - \frac{(\omega_{\text{pe}}/\omega_{\text{ce}})^2[(\omega/\omega_{\text{ce}})^2 - (\omega_{\text{pe}}/\omega_{\text{ce}})^2]}{(\omega/\omega_{\text{ce}})^2[(\omega/\omega_{\text{ce}})^2 - (\omega_{\text{uh}}/\omega_{\text{ce}})^2]}. \tag{101}$$

We will investigate the case when $\omega_{\text{uh}}/\omega_{\text{ce}} = 4$ from which it follows that $\omega_{\text{pe}}/\omega_{\text{ce}} = \sqrt{15}$. We also use the ratio $c/v_{\text{th,e}} = 50$ between the speed of light and the electron thermal velocity. Eq. (101) is solved for $\omega/\omega_{\text{ce}}$ and displayed in Fig. 3(a). For large k, the fast X wave approaches the dispersion curve of light in vacuum.

The slow X wave approaches the upper hybrid oscillation with frequency $\omega = \omega_{\text{uh}}$ for large k. In the extreme short wave length limit (large k), thermal and kinetic effects are important, and the slow X wave goes smoothly over to one of the electron Bernstein waves [24].

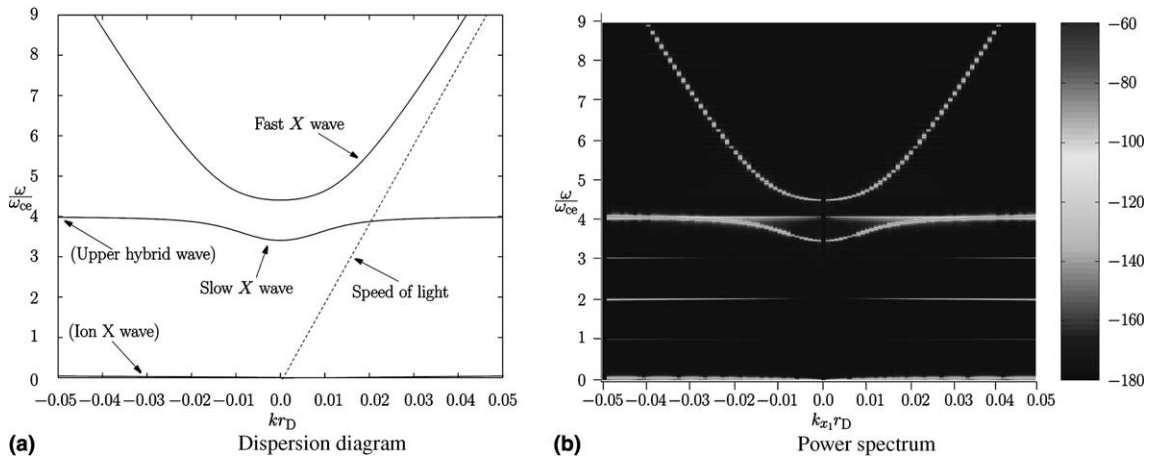

Fig. 3. Dispersion diagram for the high frequency electromagnetic extraordinary mode, obtained from cold plasma fluid theory, and power spectrum (decibel) of the transverse part E_2 of the electric field obtained from Vlasov simulation; $\omega_{uh} = 4\omega_{ce}$. (a) Dispersion diagram. (b) Power spectrum.

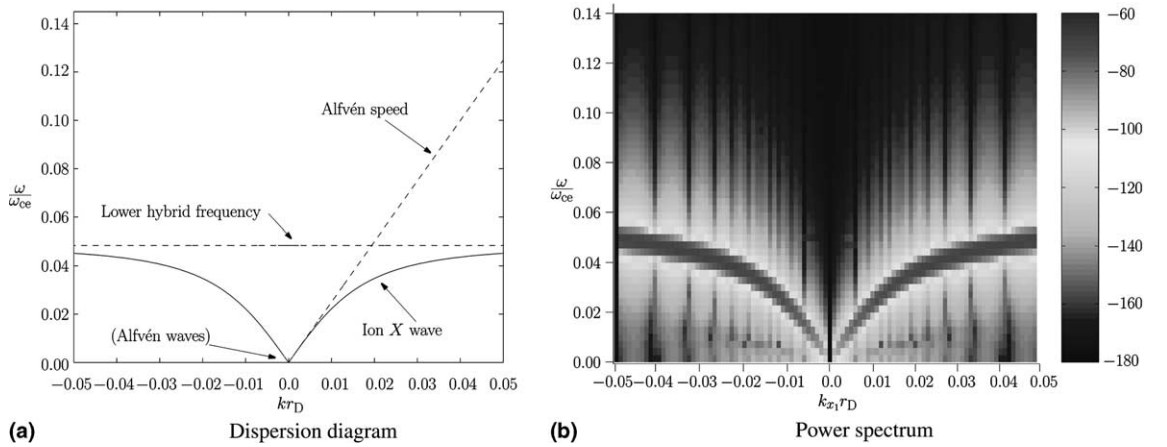

Fig. 4. Dispersion diagram for the ion extraordinary wave, obtained from cold plasma fluid theory, and power spectrum (decibel) of the transverse part E_2 of the electric field obtained from the Vlasov simulation. The waves go over to Alfvén waves at small k_{x_1} and to lower hybrid hybrid oscillations at large k_{x_1}; $\omega_{uh} = 4\omega_{ce}$, $m_i/m_e = 400$. (a) Dispersion diagram. (b) Power spectrum.

An approximate dispersion law for low frequency electromagnetic waves perpendicular to the magnetic field, obtained from a fluid description of cold ions and electrons [14], is given by

$$\frac{c^2k^2}{\omega^2}\left(\frac{\omega_{ci}^2-\omega^2+\omega_{pi}^2}{\omega_{ci}^2-\omega^2}+\frac{\omega_{pe}^2}{\omega_{ce}^2}\right)=\left(\frac{\omega_{ci}^2-\omega^2+\omega_{pi}^2}{\omega_{ci}^2-\omega^2}+\frac{\omega_{pe}^2}{\omega_{ce}^2}\right)^2-\left(\frac{\omega_{pi}^2\omega}{\omega_{ci}\left(\omega_{ci}^2-\omega^2\right)}\right)^2, \tag{102}$$

where $\omega_{pi} = \sqrt{e^2n_0/\varepsilon_0 m_e}$ is the *ion plasma frequency* and $\omega_{ci} = eB_{ext}$ is the *ion cyclotron frequency*. For numerical efficiency we use the mass ratio $m_i/m_e = 400$ between the ion and electron masses, which gives the ratios $\omega_{pi}/\omega_{ce} = \sqrt{15}/20$ and $\omega_{ci}/\omega_{ce} = 1/400$. Eq. (102) is solved for ω/ω_{ce} and displayed in Fig. 4(a). For large k_{x_1}, the dispersion curve approaches the *lower hybrid frequency* ω_{lh}, approximately given by

$$\omega_{\rm lh}^{-2} = \omega_{\rm pi}^{-2} + (\omega_{\rm ci}\omega_{\rm ce})^{-1} \tag{103}$$

and which is indicated in Fig. 4(a). For very small k_{x_1} (and low ω), the dispersion curve approaches the dispersion curve for Alfvén waves, which is given approximately by

$$\frac{\omega^2}{k^2} = \frac{c^2\omega_{\rm ci}^2}{\omega_{\rm pi}^2} \tag{104}$$

also indicated in Fig. 4(a).

The kinetic dispersion laws for electromagnetic Bernstein waves in a hot plasma have been treated by Puri et al. [24], who compare the fully kinetic and electromagnetic dispersion laws with the dispersion laws obtained by the electrostatic and cold plasma approximations. One electromagnetic effect is that each electrostatic electron Bernstein modes will split into two branches in the fully electromagnetic case.

A numerical experiment was set up with the same physical parameters as above. The power spectra for the transverse part E_2 of the electric field are displayed in Figs. 3(b) and 4(b), where the latter spectrum is a closeup of the low frequency components. The energy for the high frequency waves in Fig. 3(b) is concentrated at the linear dispersion curves for the fast and slow X modes, displayed in Fig. 3(a), in good agreement with theory. In Fig. 3(b), one can also see some weakly excited waves near the gyro harmonics $\omega/\omega_{\rm ce} \approx 1, 2, 3, 4$, which are waves not covered by the dispersion curves in Fig. 3(a), obtained from the cold plasma fluid model. The weakly excited mode at $\omega/\omega_{\rm ce} \approx 1$ is an electromagnetic effect which does not exist in the electrostatic case [24]. The energy spectrum for the low frequency waves in Fig. 4(b) shows good similarity with the dispersion curve for the low frequency wave in Fig. 4(a). The width of the energy bands in the power spectrum is the frequency resolution obtained in the simulation; a longer simulation would resolve the waves more. The frequencies of the waves in Fig. 4(b) for large k is slightly higher than the corresponding frequencies in the dispersion diagram in Fig. 4(a), which probably is a thermal effect, not included in the cold plasma fluid model.

The parameters used in the numerical simulation in the present section are as follows: The simulation domain was restricted to one spatial dimension, x_1, and two velocity dimensions, plus time. The spatial domain was set to $0 \leqslant x_1 \leqslant 2000\pi$. For the electron Vlasov equation $0 \leqslant \eta_1 \leqslant 10$ and $-10 \leqslant \eta_2 \leqslant 10$ and for the ion Vlasov equation $0 \leqslant \eta_1 \leqslant 200$ and $-200 \leqslant \eta_2 \leqslant 200$. The number of intervals was set to $N_{x_1} = 100$, $N_{\eta_1} = 30$ and $2N_{\eta_2} = 60$. The initial conditions on the particle densities were set to a sum of waves with all possible wave numbers. The initial condition for electrons was set to

$$\widehat{f}_{\rm e}(x_1, x_2, \eta_1, \eta_2, 0) = n(x)\widehat{f}_{\rm e,0}(\eta_1, \eta_2) \tag{105}$$

and for ions

$$\widehat{f}_{\rm i}(x_1, x_2, \eta_1, \eta_2, 0) = n(x)\widehat{f}_{\rm i,0}(\eta_1, \eta_2), \tag{106}$$

respectively. The density perturbation for both ions and electrons was set to

$$n(x) = \left[1 + A\sum_{i_1=1}^{49} i_1 \sin(0.05 i_1 x_1)\right] \tag{107}$$

with the relative amplitude set to $A = 10^{-7}$ so that the problem is close to linear. and the velocity distribution for electrons and ions was set to a Maxwellian in the Fourier transformed velocity space

$$\widehat{f}_{\rm e,0}(\eta_1, \eta_2) = \frac{1}{(2\pi)^2}\exp\left[-\frac{1}{2}(\eta_1^2 + \eta_2^2)\right] \tag{108}$$

and

$$\widehat{f}_{\mathrm{i},0}(\eta_1,\eta_2)=\frac{1}{(2\pi)^2}\exp\left[-\frac{1}{2}(\eta_1^2+\eta_2^2)\left(\frac{v_{\mathrm{th,e}}}{v_{\mathrm{th,i}}}\right)^{-2}\right], \tag{109}$$

respectively. The number of time steps taken was $N_t = 97280$; the end time was $t_{\mathrm{end}} = 8340$. No numerical dissipation was used. The ion-electron mass ratio was $m_{\mathrm{i}}/m_{\mathrm{e}} = 400$ and the ion and electron temperatures were set equal, $T_{\mathrm{i}} = T_{\mathrm{e}}$, giving the factor $(v_{\mathrm{th,e}}/v_{\mathrm{th,i}})^{-2} = 1/400$ in Eq. (109).

5. Conclusions

The numerical algorithm for solving the two-dimensional electrostatic Vlasov–Poisson system for electrons, has been generalised to the full Vlasov–Maxwell system for electrons and ions. The problem of the conservation of the electric and magnetic divergences has been solved by using the Lorentz potentials, written in a form which conserves the divergences at all times, and therefore a numerical scheme conserves the divergences up to the local truncation error of the scheme. Numerical test were performed and the numerical results were compared with known theory, verifying that electromagnetic effects and the motion of electrons and ions are simulated correctly. We want to point out that there seems not to be any restrictions preventing the method to be extended to the fully three-dimensional Vlasov–Maxwell system. The crucial point is to find stable outflow boundary conditions in the Fourier transformed, three-dimensional velocity space, which is a subject of future research.

6. Distribution of the computer code

The Fortran 90 code which has been used to produce the numerical results in the present article can be downloaded from the Web site http://www.tp4.ruhr-uni-bochum.de/~bengt.

Acknowledgements

This work was performed in the framework of the EU project HPRN-2001-0314, "Turbulent Boundary Layers in Geospace Plasmas." It has also been financially supported by the Swedish National Graduate School in Scientific Computing (NGSSC) and the Swedish Research Council (VR). The numerical tests were performed on the computer systems at the Department of Information Technology, Scientific Computing, Uppsala, and at the Department of Astronomy and Space Physics, Uppsala.

References

[1] T.P. Armstrong, R.C. Harding, G. Knorr, D. Montgomery, Solution of Vlasov's equation by transform methods, in: Methods in Computational Physics, vol. 9, Academic Press, New York, 1970, pp. 29–86.
[2] F. Assous, P. Degond, E. Heintze, P.A. Raviart, J. Segre, On a finite-element method for solving the three-dimensional Maxwell equations, J. Comput. Phys. 109 (2) (1993) 222–237.
[3] C.K. Birdsall, A.B. Langdon, Plasma Physics via Computer Simulation, McGraw-Hill Inc., 1985, ISBN 0-07-005371-5.
[4] F.F. Chen, Introduction to Plasma Physics, second ed., Plasma Physics, vol. 1, Plenum Press, New York, 1984, ISBN 0-306-41332-9.
[5] C.Z. Cheng, The integration of the Vlasov equation for a magnetized plasma, J. Comput. Phys. 24 (1977) 348–360.
[6] C.Z. Cheng, G. Knorr, The integration of the Vlasov equation in configuration space, J. Comput. Phys. 22 (1976) 330–351.

[7] J. Denavit, W.L. Kruer, Comparison of numerical solutions of the Vlasov equation with particle simulations of collisionless plasmas, Phys. Fluids (1971) 1782–1791.
[8] J.W. Eastwood, The virtual particle electromagnetic particle-mesh method, Comput. Phys. Commun. 64 (1991) 252–266.
[9] F. Edelvik, Hybrid Solvers for the Maxwell Equations in Time-Domain. The Department of Information technology, Uppsala University. Doctoral thesis. (Uppsala Dissertations from the Faculty of Science and Technology), ISSN 1104-2516, ISBN 91-554-5354-6. Downloadable from Web site http://publications.uu.se/theses/, 2002.
[10] B. Eliasson, Outflow boundary conditions for the Fourier transformed one-dimensional Vlasov–Poisson system, J. Sci. Comput. 16 (1) (2001) 1–28.
[11] B. Eliasson, Outflow boundary conditions for the Fourier transformed two-dimensional Vlasov equation, J. Comput. Phys. 181 (2002) 98–125.
[12] J. Feng, W.N.G. Hitchon, Self-consistent kinetic simulation of plasmas, Phys. Rev. E 61 (1999) 3160–3173.
[13] F. Filbet, E. Sonnedrücker, P. Bertrand, Conservative numerical schemes for the Vlasov equation, J. Comput. Phys. 172 (2001) 166–187.
[14] R.J. Goldston, P.H. Rutherford, Introduction to Plasma Physics, Institute of Physics Publishing, Bristol and Philadelphia, 1997, ISBN 0-7503-0183-X.
[15] B. Gustafsson, H.-O. Kreiss, J. Oliger, Time Dependent Problems and Difference Methods, Wiley, New York, 1999, ISBN 0-471-50734-2.
[16] J.D. Jackson, Classical Electrodynamics, third ed., Wiley, New York, 1999, ISBN 0-471-30932-X.
[17] B. Jiang, J. Wu, L.A. Povinelli, The origin of spurious solutions in computational electromagnetics, J. Comput. Phys. 125 (1996) 104–123.
[18] A.J. Klimas, W.M. Farrel, A splitting algorithm for Vlasov simulation with filamentation filtration, J. Comput. Phys. 110 (1994) 150–163.
[19] A.J. Klimas, A method for overcoming the velocity space filamentation problem in collisionless plasma model solutions, J. Comput. Phys. 68 (1987) 202–226.
[20] S.K. Lele, Compact finite difference schemes with spectral-like resolution, J. Comput. Phys. 103 (1992) 16–42.
[21] A. Mangeney, F. Califano, C. Cavazzoni, P. Travnicek, A numerical scheme for the integration of the Vlasov–Maxwell system of equations, J. Comput. Phys. 179 (2002) 495–538.
[22] B. Marder, A method for incorporating Gauss' law into electromagntetic PIC codes, J. Comput. Phys. 68 (1987) 48–55.
[23] R.L. Morse, C.W. Nielson, Numerical simulation of the Weibel instability in one and two dimensions, Phys. Fluids 14 (4) (1971) 830–840.
[24] S. Puri, F. Leuterer, M. Tutter, Dispersion curves for generalised Bernstein modes, J. Plasma Phys. 9 (1) (1973) 89–100.
[25] L. Råde, B. Westergren, BETA Mathematics Handbook, second ed., Studentlitteratur AB, Lund, Sweden, 2002.
[26] J.C. Strikwerda, Finite Difference Schemes and Partial Differential Equations, Wadsworth Inc, 1989 (Chapter 1.6).
[27] S.H. Strogatz, Nonlinear Dynamics and Chaos, Addison-Wesley Publishing Company, 1994.
[28] B. Thidé, Electromagnetic Field Theory. Web book, downloadable from Web site: http://www.plasma.uu.se/CED/Book, 2002.
[29] C.L. Wagner, J.B. Schneider, Divergent fields, charge, and capacitance in FDTD simulations, IEEE Transactions on Microwave Theory and Techniques 46 (12) (1998) 2131–2136.
[30] R. Wangsness, Electromagnetic Fields, second ed., Wiley, New York, 1986.